

Curvature- and Phase-Induced Protein Sorting Quantified in Transfected Cell-Derived Giant Vesicles

Guillermo Moreno-Pescador,[†] Christoffer D. Florentsen,[†] Henrik Østbye,[‡] Stine L. Sønder,[§] Theresa L. Boye,[§] Emilie L. Veje,[†] Alexander K. Sonne,[†] Szabolcs Semsey,[†] Jesper Nylandsted,^{§,||} Robert Daniels,[‡] and Poul Martin Bendix^{*,†,ID}

[†]Niels Bohr Institute, University of Copenhagen, DK-2100 Copenhagen, Denmark

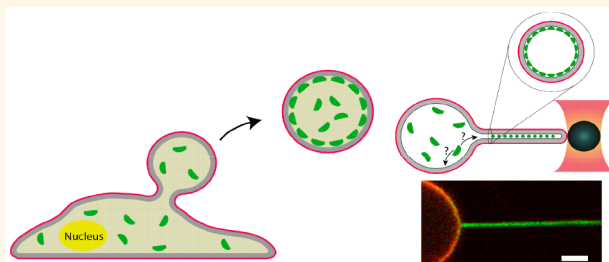
[‡]Department of Biochemistry and Biophysics, Stockholm University, 10691 Stockholm, Sweden

[§]Membrane Integrity Group, Unit for Cell Death and Metabolism, Center for Autophagy, Recycling and Disease, Danish Cancer Society Research Center, Strandboulevarden 49, DK-2100 Copenhagen, Denmark

^{||}Department of Cellular and Molecular Medicine, Faculty of Health Sciences, University of Copenhagen, DK-2200 Copenhagen N, Denmark

Supporting Information

ABSTRACT: Eukaryotic cells possess a dynamic network of membranes that vary in lipid composition. To perform numerous biological functions, cells modulate their shape and the lateral organization of proteins associated with membranes. The modulation is generally facilitated by physical cues that recruit proteins to specific regions of the membrane. Analyzing these cues is difficult due to the complexity of the membrane conformations that exist in cells. Here, we examine how different types of membrane proteins respond to changes in curvature and to lipid phases found in the plasma membrane. By using giant plasma membrane vesicles derived from transfected cells, the proteins were positioned in the correct orientation and the analysis was performed in plasma membranes with a biological composition. Nanoscale membrane curvatures were generated by extracting nanotubes from these vesicles with an optical trap. The viral membrane protein neuraminidase was not sensitive to curvature, but it did exhibit strong partitioning (coefficient of $K = 0.16$) disordered membrane regions. In contrast, the membrane repair protein annexin 5 showed a preference for nanotubes with a density up to 10–15 times higher than that on the more flat vesicle membrane. The investigation of nanoscale effects in isolated plasma membranes provides a quantitative platform for studying peripheral and integral membrane proteins in their natural environment.



KEYWORDS: plasma membrane proteins, annexin, neuraminidase, membrane curvature, nanotubes, phase sorting, giant plasma membrane vesicles

Organization of membrane proteins is tightly regulated in cells through both chemical and physical factors. Recent evidence suggests that membrane shape can influence protein recruitment and be amplified by proteins with specific shapes.^{1–3} Peripheral membrane-binding proteins can alter the curvature of a membrane in a specific direction by associating with one side of the lipid bilayer.^{4–9} In model membranes, several types of proteins with curved molecular-binding sites, or hydrophobic amphiphatic motifs, have been found to sense membrane curvatures (MCs).^{2,8,10–15} This MC sensing property constitutes a built-in recruitment function for these proteins, which drives them to highly curved regions of the membrane or depletes them from regions having

unfavorable MCs. In cells, peripheral membrane-binding proteins with this capacity have been proposed to play a major role in shaping the cell surface as well as the endocytic vesicles.⁸ At high density, membrane proteins can also form a mechanical scaffold that shapes or supports the membrane.^{8,16,17} Investigations of the dynamic interplay between proteins and the native plasma membrane (PM) requires that the proteins possess the correct orientation in the membrane

Received: February 6, 2019

Accepted: June 5, 2019

Published: June 5, 2019

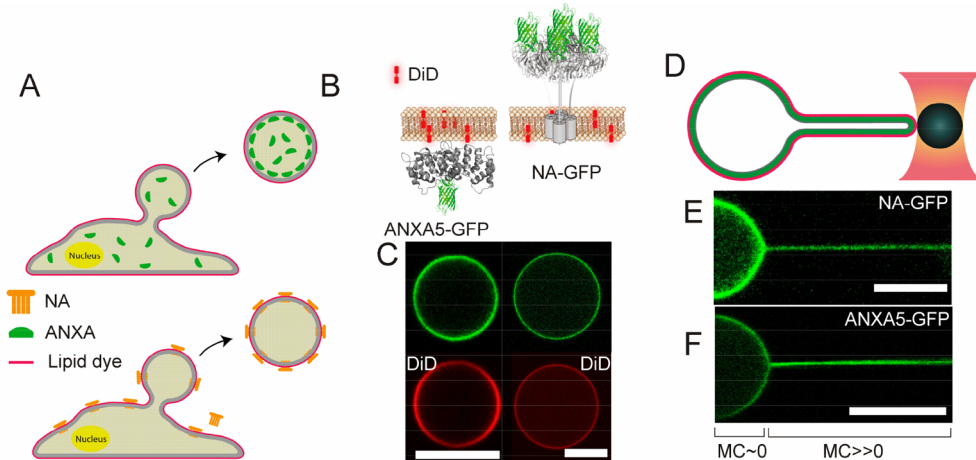


Figure 1. Optical manipulation of plasma-membrane-derived vesicles from transfected cells expressing different types of membrane proteins fused to a fluorescent protein for visualization. (A) Cells expressing different types of fluorescent membrane proteins are labeled with a lipid dye (DiD) and treated with *N*-ethylmaleimide to cause vesiculation of the PM. (B) Structures displaying the correct orientation or localization of the tetrameric integral membrane protein influenza NA (PDB: 3T1S) and the peripheral-binding membrane protein ANXA5 (PDB: 1a8a) with respect to the PM. The stalk and transmembrane domain linking NA to the PM are not present in the structure, and the structures for GFP were added manually to highlight that the assays involve the use of fusion proteins. (C) PM vesicles containing ANXA5-GFP (top left) or NA-GFP (top right) and visualization of the membrane with DiD (bottom). (D) Schematic of the experimental setup used to optically manipulate PM vesicles. An optically trapped bead with a point contact to the vesicle membrane is used to pull nanotubes with a diameter below the diffraction limit of light. (E) Nanotubes extracted from PM vesicles containing NA-GFP or ANXA5-GFP are shown. The low and high membrane curvature (MC) regions are indicated below the images. Scale bars are 10 μ m.

or, in the case of peripheral membrane proteins, are located at the correct side of the membrane.

Membrane shaping has been extensively studied in simple model systems where the lipid composition is well-defined, but model membranes do not necessarily represent the properties of the complex plasma membrane of living cells.^{4,5,7,12,18–22} Similarly, recruitment of membrane proteins to highly curved membranes has been investigated in model membrane systems on tubes extracted from giant unilamellar lipid vesicles (GUVs).^{8,11} A caveat to these approaches is that transmembrane proteins reconstituted in GUVs are randomly oriented and thus do not faithfully represent the complexity of the PM. Another difficulty persists in the study of peripheral membrane proteins that bind to the cytoplasmic side of the membrane, as these need to be encapsulated inside the GUV, a process that is inherently difficult and requires either removal of the remaining external protein or inhibition of protein binding on the outside of the GUV.¹⁵

More recently, living cells have been employed to investigate the dynamics of proteins in curvature gradients and with regard to lipid-order preference into nanoscale domains.²³ The membrane curvature sensing of a G-protein-coupled receptor was investigated in cells by extracting lipid nanotubes from the PM with diameters of ~20–100 nm.¹⁰ However, only cells exhibiting a low degree of actin polymerization into the lipid tube can be used for such studies and the tubes have to be extended up to ~50 μ m to possess biologically relevant high MC.^{10,24} Long cellular tubes can also exhibit slow mixing with the PM on the cell body, and it is unknown how the actin cortex, at the cell–tube junction, affects the mixing of proteins between the PM on the cell body and the tube. Finally, for quantification of curvature sorting, a reference area consisting of a flat membrane is needed to calculate the relative increase of protein density on the curved region. Such flat areas are difficult to identify with light microscopy due to the abundance

of the ruffled and polymorphic PM shapes which exists at the nanoscale in living cells.

We have developed a platform to investigate nanoscale protein dynamics at the PM using cell-derived vesicles, which provide a natural milieu comprising the complex lipid environment and the crowded population of properly oriented proteins. The preference of internally bound, or integral membrane proteins, for lipid domains can be elucidated in plasma membrane vesicles by clustering nanoscale domains into larger phases that can be resolved by microscopy. Optical extraction of lipid nanotubes from cell-derived PM vesicles allows control over membrane curvature, and we show how the relative protein density on the inner side of lipid tubes can be quantitatively compared to the density on the nearly flat surface of the PM vesicle membrane. Here, we used this platform to study several peripheral associating membrane proteins from the annexin family and the integral membrane protein influenza neuraminidase. Our results demonstrate how the membrane-repair protein, annexin A5 (ANXA5), strongly enriches within nanotubes with negative MC, whereas ANXA2 does not share this preference. The different ability between these two cognate and quite similarly shaped proteins in sensing membrane curvatures appears linked to the different ability of these proteins to form trimers or larger protein assemblies on the membrane. Oligomerization of ANXA5 is supported by mobility measurements on the tubes, which show that ANXA5 and its closely related family member, ANXA4, can possess extremely low mobility compared to that of ANXA2. In contrast, influenza NA did not show a curvature affinity but was found to partition to disordered lipid regions in the membrane.

RESULTS AND DISCUSSION

Formation of PM Vesicles with Properly Orientated Membrane Proteins.

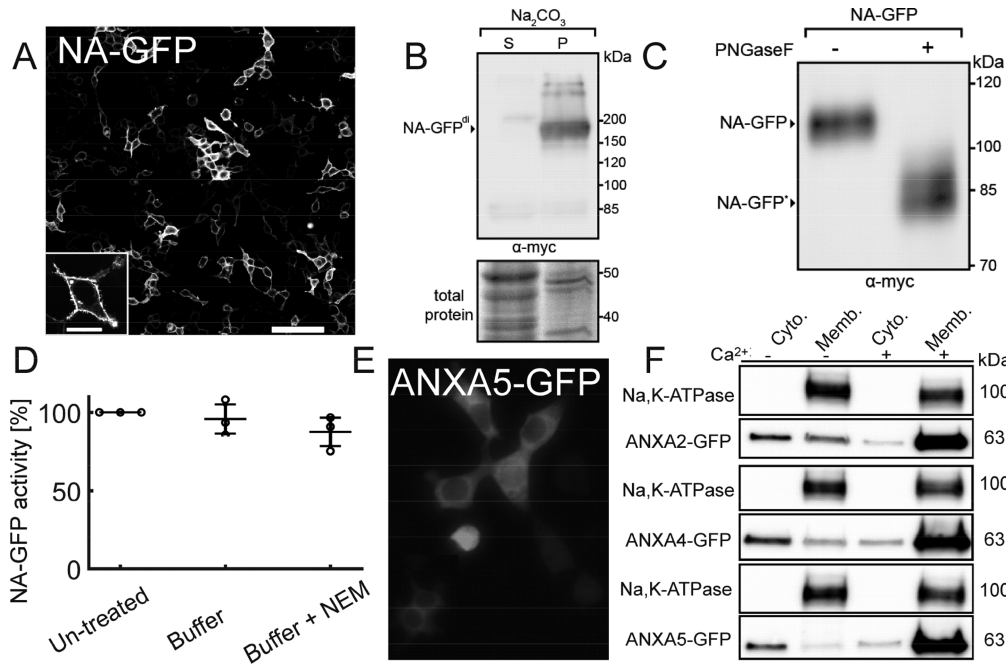


Figure 2. Property analysis of NA-GFP and ANXA5-GFP in cells. (A) Confocal image of transfected cells expressing NA-GFP shows that the protein is primarily located at the cell periphery. Scale bar is 100 μm . Inset shows a magnified view of a single cell. Scale bar is 20 μm . (B) NA-GFP immunoblots of cell-derived vesicles that were treated with Na_2CO_3 and subjected to ultracentrifugation to separate the integral membrane proteins (P) from the cytosolic and peripheral membrane proteins (S). An image of the amido black-stained membrane is included as a control for the fractionation. NA-GFP was expressed with a C-terminal myc tag for detection. (C) Lysates from cells expressing NA-GFP with a myc tag were either untreated or deglycosylated with PNGaseF prior to resolution by nonreducing sodium dodecyl sulfate polyacrylamide gel electrophoresis (SDS-PAGE) and immunoblotting. (D) Sialidase activity of NA-GFP was measured after the addition of the vesiculation buffer with and without NEM and compared to untreated cells. The activity measurements were made using equal numbers of transfected cells, and the untreated samples were set to 100%. Error bars denote the standard deviation of three experiments, and the mean is indicated by the horizontal line. (E) Confocal image showing that ANXA5-GFP is uniformly distributed throughout the cytoplasm. (F) Representative fractionation experiment of plasma membrane vesicles extracted from HEK293T cells transiently transfected with ANXA2-GFP, ANXA4-GFP, or ANXA5-GFP. Membrane vesicles were permeabilized with digitonin $\pm \text{Ca}^{2+}$ before fractionation by centrifugation. Immunoblot analysis was carried out using ANXA2, ANXA4, and ANXA5 antibodies. Na,K-ATPase served as an integral membrane protein control. Cyto: cytosolic fraction. Memb: membrane fraction. Extended blots are presented in Figure S3.

proteins constitute two classes of proteins with distinct plasma membrane interactions. In order to use optical manipulation methods to investigate the curvature and phase affinity of these two classes of proteins in isolated PM vesicles, different substrate proteins were examined. For peripheral-binding membrane proteins, we chose to analyze different annexin proteins because all of the family members share a core domain with a convex shape that can potentially act as a sensor for negative PM curvatures. In addition, annexin family members possess different membrane-binding and oligomerization properties, which enables them to function in many cellular processes including cell membrane repair.^{4,25} As an integral membrane protein, we chose to examine the influenza glycoprotein neuraminidase (NA) due to the asymmetric shape of its tetrameric conformation and previous reports suggesting it clusters into lipid rafts²⁶ and regions of curvature on the plasma membrane.^{27,28} During infection, NA promotes the mobility of influenza viruses by removing extracellular sialic acid receptors and the structural asymmetry is attributed to the large enzymatic head domain, which is linked to the membrane by a long stalk connected to an N-terminal transmembrane domain.²⁹

To visualize the proteins and increase the likelihood that they possessed the correct orientation with respect to the membrane, each protein was transiently expressed in HEK293T cells with a C-terminal fluorescent reporter such

as green fluorescent protein (GFP) (see Figure 1A,B). The PM was labeled by the addition of vybrant DiD to the cell culture medium, and the PM vesicles were then generated by treating the HEK293T cells (24 h post-transfection for ANXA and 48 h for NA) with N-ethylmaleimide (NEM) for 2 h followed by gentle shaking.³⁰ The solution containing the PM vesicles was harvested, and the vesicles were immobilized on a poly-L-lysine-coated surface. This setup enabled each protein to be visualized with respect to the membrane (Figure 1C) for subsequent optical manipulations for testing partitioning and mobility of proteins between low and high membrane curvatures by pulling nanotubes (Figure 1D–F).

Prior to manipulating the samples, a number of methods were used to examine if the C-terminal tags affected the folding, localization, orientation, or membrane-binding properties of each protein. Confocal imaging (Figure 2A), NaCO_3 extractions (Figure 2B), and deglycosylation of N-linked glycans that are added in the lumen of the endoplasmic reticulum (Figure 2C) all confirmed that NA-GFP primarily localized to the PM as expected and was integrated into the membrane with the correct orientation.³¹ The sialidase activity of NA-GFP was also largely unaffected by the procedure for inducing PM vesicle formation, indicating it retained the appropriate tetrameric conformation (Figure 2D). Cell imaging revealed that ANXA5-GFP mainly localized to the cytoplasm (Figure 2E), and it remained nonmembrane

associated during the PM vesicle formation until late stages of the PM vesiculation (Figure S1A–C). These results indicated that either the Ca^{2+} concentration is too low to promote the membrane association of ANXA5 or that the GFP tag interferes with the binding. To investigate this more directly, the integrity of the transfected cell membranes was disrupted with digitonin to allow extracellular Ca^{2+} influx, and the membrane association was determined. The influx of Ca^{2+} caused ANXA5-GFP as well as ANXA2-GFP and ANXA4-GFP to associate with the membrane, indicating the GFP does not prevent ANXA binding. Vesicles were also isolated from cells expressing different types of GFP-tagged membrane proteins. ANXA1, ANXA2, ANXA4, and ANXA5 were all transiently expressed in HEK293T cells and found to be membrane bound in PM vesicles (Figure S2). To verify that the PM vesicles allow influx of Ca^{2+} , ultimately leading to membrane binding of ANXA5, we substituted the CaCl_2 in the vesiculation buffer with MgCl_2 , and ANXA5-GFP only showed a luminal distribution (Figure S1E). These results are consistent with the finding that intracellular Ca^{2+} concentrations in living cells lead to mostly cytosolic unbound ANXA5, but if the membrane integrity is lost by a membrane rupture, the influx of Ca^{2+} results in ANXA5 (and other annexins) binding to the PM and consequent resealing of the membrane.⁴

ANXA4 and ANXA5 have been found to bind locally around cellular membrane ruptures during influx of Ca^{2+} , and recently, it was shown that ANXA4, ANXA5, and ANXA6 are all important in sealing membranes upon laser-induced membrane rupture.^{4,25} The threshold Ca^{2+} level for facilitating binding could well be affected by MC. Future studies will show if the threshold level of Ca^{2+} , which facilitates binding, can be shifted by MC (Figure S4).

Next, we used a protease susceptibility assay to assess if the process of vesicle formation affects the location and orientation of the proteins. When proteinase K (co-injected with Alexa Hydrazide 633 as a marker) was added to PM vesicles containing ANXA5-GFP, only a slow loss of GFP signal was observed due to bleaching (Figure 3A,B). In contrast, when recombinant ANXA5-GFP was added to the exterior side of the isolated PM vesicles, the GFP signal was completely lost following treatment with proteinase K (Figure S5), indicating that the transiently expressed ANXA5-GFP was bound to the inner leaflet of the PM vesicles. Proteinase K addition also resulted in the loss of the GFP signal from PM vesicles containing NA-GFP, confirming that the large enzymatic head domain is positioned on the exterior side of the vesicles (Figure 3C,D). Together, these results show that the correct orientation and the location of the transiently expressed proteins are preserved in the isolated PM vesicles.

Although the formation of PM vesicles results in some loss of membrane asymmetry, as indicated by ANXA binding to the outer leaflet (Figures S5 and S6),³⁰ the proteins, however, associated with the PM vesicles do retain their correct orientation, indicating that the protein composition of the PM vesicles is likely not affected. The PM vesicle assay therefore allows full control over protein location and orientation for both membrane-binding proteins and integral membrane proteins, which is in striking contrast to other model systems like protein reconstituted GUVs.^{11,32} Additionally, the PM vesicles are devoid of internal cellular structures³³ and therefore can be used to study the interplay between the PM and protein dynamics.

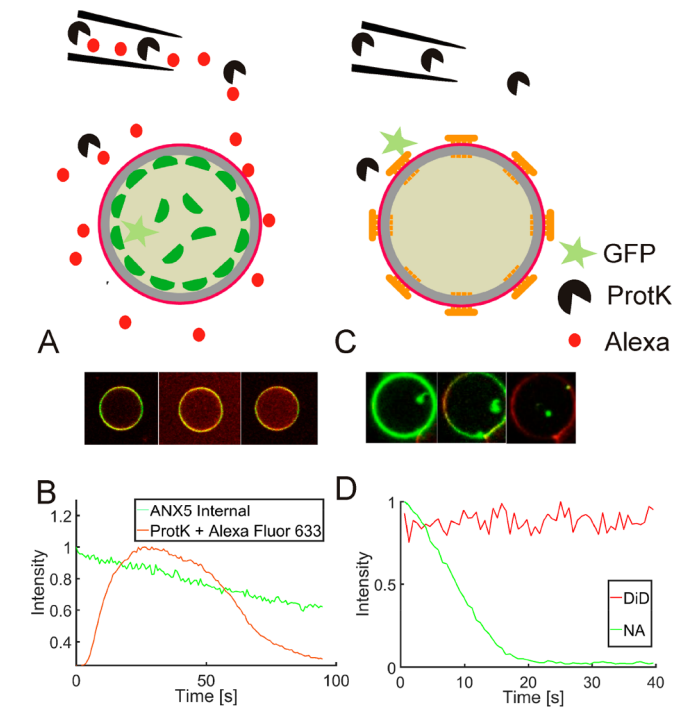


Figure 3. Protein orientation is retained in the PM vesicles isolated from the transfected cells. (A) Confocal imaging was used to monitor the fluorescence intensity of ANXA5-GFP in the PM vesicles before and after the addition of proteinase K by a micropipette that contained Alexa Fluor 633 as an indicator. (B) Graphs displaying the time-dependent quantification of the ANXA5-GFP and Alexa Fluor 633 intensities that were measured. The slight decrease in GFP intensity is likely attributed to bleaching. (C) Images of DiD-labeled PM vesicles containing NA-GFP before and after the addition of proteinase K for different times. (D) Graphs displaying the intensities of the NA-GFP signal and the lipid dye DiD that were obtained at the indicated times following the addition of proteinase K.

Phase-Dependent Partitioning of Peripheral Binding and Integral Membrane Proteins. PMs comprise different lipids that form nanoscale environments with varying degrees of lipid order that can impart a localization bias on membrane proteins. Due to technical limitations, most studies on protein partitioning between fluid-ordered and disordered phases have examined integral membrane proteins or proteins that bind to the external leaflet of the PM.^{34–37} The production of PM vesicles from transfected cells overcomes some of the limitations for investigating how proteins laterally organize on the internal side of the PM as the expressed GFP-tagged cytosolic proteins remain encapsulated by the PM. To investigate this potential application, we examine the phase separation of NA-GFP, which has previously been reported to partition into lipid-ordered “raft” domains by detergent-resistant methods.^{26,38,39}

To induce and visualize the phase separation, PM vesicles were cooled to ~ 10 °C and treated with cholera toxin B (CTxB) labeled with Alexa 647. CTxB cross-links gangliosides (GM1) in nanoscopic PM-ordered regions, resulting in their coalescences into large domains that are resolvable by fluorescent microscopy.³⁰

We next tested the ability of PM vesicles to sort large and asymmetric transmembrane proteins between ordered and less ordered phases. For the investigation of NA phase preference,

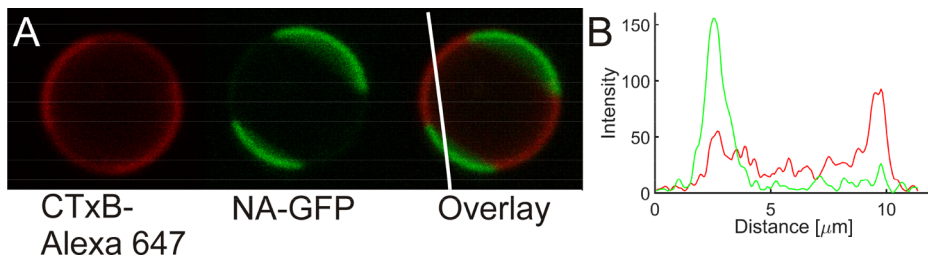


Figure 4. Phase-induced segregation of integral proteins in PM vesicles. Upon cooling to $\sim 10\text{ }^{\circ}\text{C}$, the PM vesicles undergo phase segregation. (A) Phase-segregated vesicle derived from a HEK293T cell expressing NA-GFP (green) and treated with cholera toxin B (CTxB, red). NA-GFP is found to colocalize with low CTxB-Alexa 647 signal and hence with domains having lower degree of lipid order. (B) Intensity profiles along the line shown in (A) for both the CTxB-Alexa 647 (red) and NA-GFP signal (green).

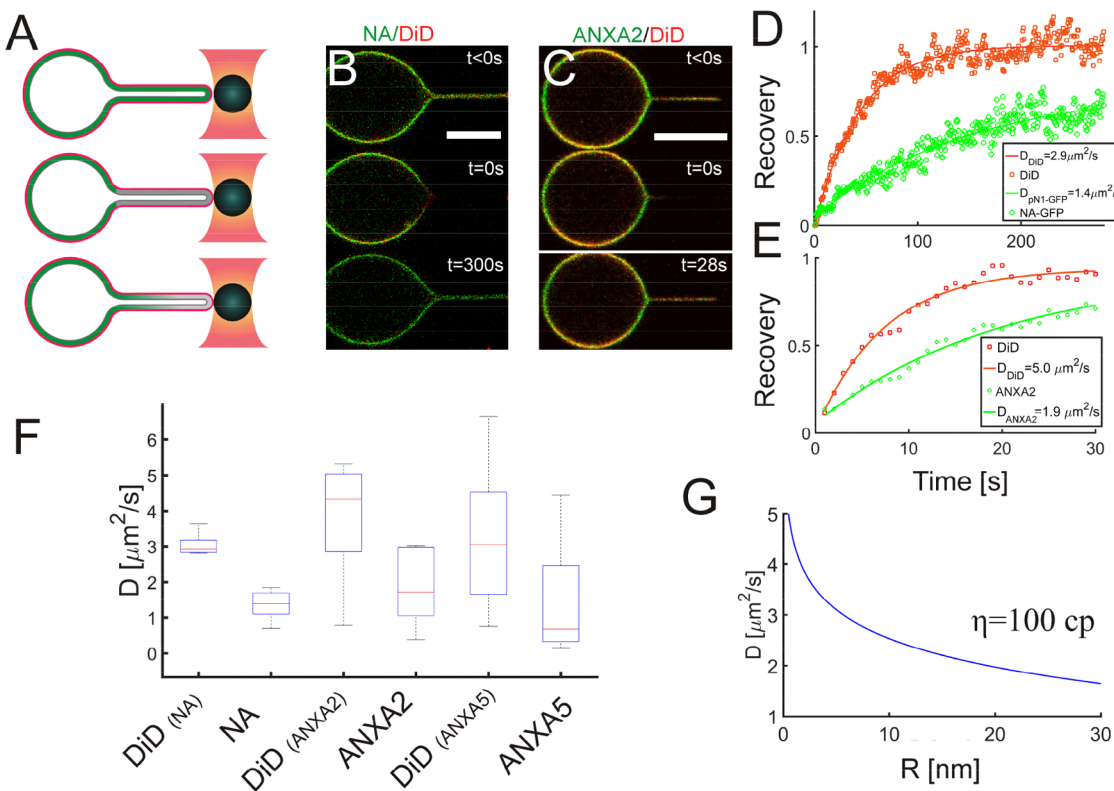


Figure 5. Mobility of membrane proteins in PM vesicles measured by performing fluorescent recovery after photobleaching (FRAP) on optically extracted nanotubes. (A) Schematic depiction of the FRAP experiment using PM vesicles. A nanotube is extracted from a PM vesicle containing GFP-tagged proteins and the membrane label DiD. The tube is subsequently bleached by a laser for $\sim 2\text{ s}$, and the fluorescence recovery from DiD and GFP-tagged proteins is monitored by confocal microscopy. (B) Example FRAP images obtained from nanotubes extracted from a PM vesicle containing NA-GFP and DiD or (C) ANXA2-GFP and DiD at the indicated times with respect to bleaching. Scale bars are $10\text{ }\mu\text{m}$. (D) Recovery curves of NA-GFP and DiD and (E) ANXA2-GFP and DiD with exponential fits used to extract recovery times. (F) Box-and-whiskers plots showing the calculated diffusion constants for NA-GFP ($N = 8$), ANXA2-GFP ($N = 5$), ANXA5-GFP ($N = 11$), and the DiD lipid analogue measured in the presence of the respective protein. The difference in diffusion of the three proteins was not significant using the unpaired *t* test, $p > 0.05$. (G) Calculated diffusion coefficients as a function of size of the membrane inclusion predicted by the Saffmann-Delbrück model (eq 3) with membrane viscosity of 100 cP.

we used CTxB to induce lipid phase segregation to perform the first investigation of the phase preference of NA in phase-separated PM vesicles which closely resemble the PM of cells. Interestingly, NA-GFP was found to colocalize with regions of low CTxB signal, as shown in Figure 4A,B, indicating a preference for more disordered regions (see Figure S7 for additional examples). The partition coefficient between the phases defined as $K = I_{\text{ordered}}/I_{\text{disordered}}$ was found to be $K = 0.16 \pm 0.08$ ($N = 16$ vesicles) and shows a clear affinity of NA-GFP for disordered domains. This partition coefficient is similar to values found for other proteins favoring disordered phases.³⁶

This evidence of NA-GFP localization to less ordered domains is consistent with previous findings showing that non-palmitoylated membrane proteins prefer disordered domains.^{34,36,40} Viral proteins like hemagglutinin (HA) and NA have been found to colocalize into ordered raft domains by detergent-resistant methods.^{26,38,39}

HA has also been shown to partition into disorder domains in model membranes,⁴¹ contradictory to the partitioning into ordered raft-like regions in detergent-based studies.⁴² Partitioning into ordered phases of transmembrane proteins has been shown to require palmitylation of the proteins^{36,43} but is

not sufficient for targeting HA to ordered domains. Future studies could answer whether coexpression of hemagglutinin and neuraminidase in PM vesicles could affect the preference of the proteins for certain phases or whether possibly the matrix proteins M1 and M2 could play a role in partitioning of viral proteins.³⁹ Of interest here is the fact that the ion channel M2 has been shown to localize to the budding periphery in phase-separated reconstituted model membranes, corresponding to the interface of ordered and disordered domains.^{44,45} Intriguingly, it has been shown that lipids isolated from viral envelopes exist primarily in a disordered phase at physiological temperature, which could explain the preference of NA and HA for fluid phases in PM vesicles.⁴⁶

Interestingly, vesicles derived from ANXA5-GFP expressing cells showed domain formation upon cooling without addition of CTxB (see Figure S8). In these vesicles, ANXA5-GFP was found to localize to distinct regions indicated by low or high intensities of GFP signal, as shown in the 3D reconstruction in Figure S8A. ANXA5-GFP binds to phosphatidylserine lipids mediated by calcium, which indicates that the regions with high GFP signal might be enriched with anionic lipids. Overall, these results show that cooling of PM vesicles can trigger both internal and transmembrane proteins to segregate to distinct regions having different order and possibly also a different mobility.

Mobility Measurements of Proteins Inside Tubes Reveal Oligomerization of Annexins. In living cells, the actin skeleton strongly affects both lipid and membrane protein mobility.^{47,48} Therefore, it is difficult to distinguish between the contributions of the actin cortex to mobility from protein–protein associations or the binding of proteins to specific domains in the membrane. However, PM vesicles are devoid of actin filaments, making it possible to quantify the mobility of proteins and lipids in the bilayer from fluorescent recovery after photobleaching (FRAP) measurements performed on nanotubes extracted from a PM vesicle using an optical trap (Figure 5A). This configuration avoids the larger PM vesicle, which minimizes the overall phototoxic effects and ensures that the lipid mixing in the nanotube only occurs with the PM reservoir.

To perform the measurements, the PM vesicles containing either NA-GFP or different ANXA-GFPs were first labeled with the lipid analogue DiD; the nanotubes were then extracted and bleached. Following the bleaching, the fluorescence recovery of both DiD and the GFP reporter was recorded simultaneously (Figure 5B,C), and the recovery curves for the two proteins were plotted and fitted to the expression⁴⁹

$$F(t) = F_{\infty} \left(1 - \exp\left(-\frac{t}{\tau}\right) \right) \quad (1)$$

where $F(t)$ is the fluorescent intensity at time t and F_{∞} is the steady-state intensity. The recovery time constant τ is related to the diffusion constant through⁴⁹

$$D = \frac{4}{\pi^2} \frac{L^2}{\tau} \quad (2)$$

where L is the length of the tube. Based on these calculations, we determined that the diffusion constants for DiD ($\langle D \rangle = 2.8 \mu\text{m}^2/\text{s}$) was approximately 2-fold higher than the diffusion constant of NA-GFP ($\langle D \rangle = 1.4 \mu\text{m}^2/\text{s}$), indicating the large

viral protein moves slower in the membrane than the DiD lipid analogue (Figure 5F).

When similar experiments were carried out for the different ANXA-GFPs, a striking variation in behavior was observed. Whereas ANXA2-GFP ($\langle D \rangle = 1.7 \mu\text{m}^2/\text{s}$) was mobile in all experiments, we observed that the diffusion constant for ANXA5-GFP was lower ($\langle D \rangle = 0.7 \mu\text{m}^2/\text{s}$), suggesting that ANXA5-GFP became less mobile within the membrane tube (Figure 5F). However, these average diffusion constants were not found to be significantly different using the two-sample t test ($p > 0.05$). Interestingly, ANXA5-GFP also displayed differential mobility in several experiments ($N = 6$) when large ($\sim 15 \mu\text{m}$) PM vesicles were analyzed using strong bleaching conditions. On the vesicle surface, ANXA5-GFP showed full fluorescence recovery despite the bleaching conditions, but almost no recovery was observed in the nanotubes (Figure S9A), suggesting the mobility of ANXA5-GFP is affected by curvature. Somewhat in line with these observations, the diffusion constant for the DiD lipids in the presence of ANXA2-GFP ($\langle D \rangle = 4.3 \mu\text{m}^2/\text{s}$) was higher than that in the presence of ANXA5-GFP ($\langle D \rangle = 3.0 \mu\text{m}^2/\text{s}$).

The lack of ANXA5-GFP mobility in some of the experiments ($N = 16$) may reflect an underlying difference in the nanoscale organization of ANXAs. ANXA5 and ANXA4 have been reported to form trimers that assemble into large-scale 2D lattices that are capable of supporting model membranes.^{50–54} The low diffusion constants that were measured for ANXA5-GFP (Figure 5) could arise from oligomerization of ANXA5 into trimers or larger assemblies, which do not extend the whole length of the tube as they still exhibit some degree of mobility. These larger assemblies would effectively slow down diffusion, and this relationship enables the size of the aggregate to be estimated by modeling diffusion of membrane inclusions of varying lateral in-plane size, as described by Saffman and Delbrück.⁵⁵ In this equation, the diffusion constant is found to decrease logarithmically with inclusion size, R :

$$D = \frac{K_B T}{4\pi\eta_m h} \left(\ln\left(\frac{h\eta_m}{R\eta_c}\right) - \gamma \right) \quad (3)$$

where η_m and η_c are the viscosities of the membrane and solution, respectively, γ is the Euler constant ($\gamma = 0.5772$), and h is the thickness of the membrane. In Figure 5G, the diffusion constant is plotted versus the inclusion size for sizes ranging from 0.5 nm (size of a lipid) to 30 nm in radius, which corresponds to an aggregate of a few proteins, with a membrane viscosity of 100 cP that is typical for biological membranes.⁵⁶ The relation expressed in eq 3 has been shown to be valid for inclusion sizes up to $R_c = h\eta_m/(2\eta_c)$, which is well beyond the size range plotted in Figure 5G.^{55,57} When the mobilities measured for the different proteins (Figure 5F) were compared to the values predicted by eq 3, all of the experimental values were found to correspond to single proteins or small aggregates that are ~ 10 nm. The slightly lower experimental values (Figure 5F) can be explained by the crowded environment in the plasma membrane, which is not accounted for in eq 3. Additionally, the number of lipids that are bound to the protein could contribute to the lower values, as protein mobility has been shown to decrease significantly with increases in the number of bound lipids.⁵⁸ Annexins bind to negatively charged lipids with serine head groups and to phosphorolysed phosphatidylinositol lipids. Up to three

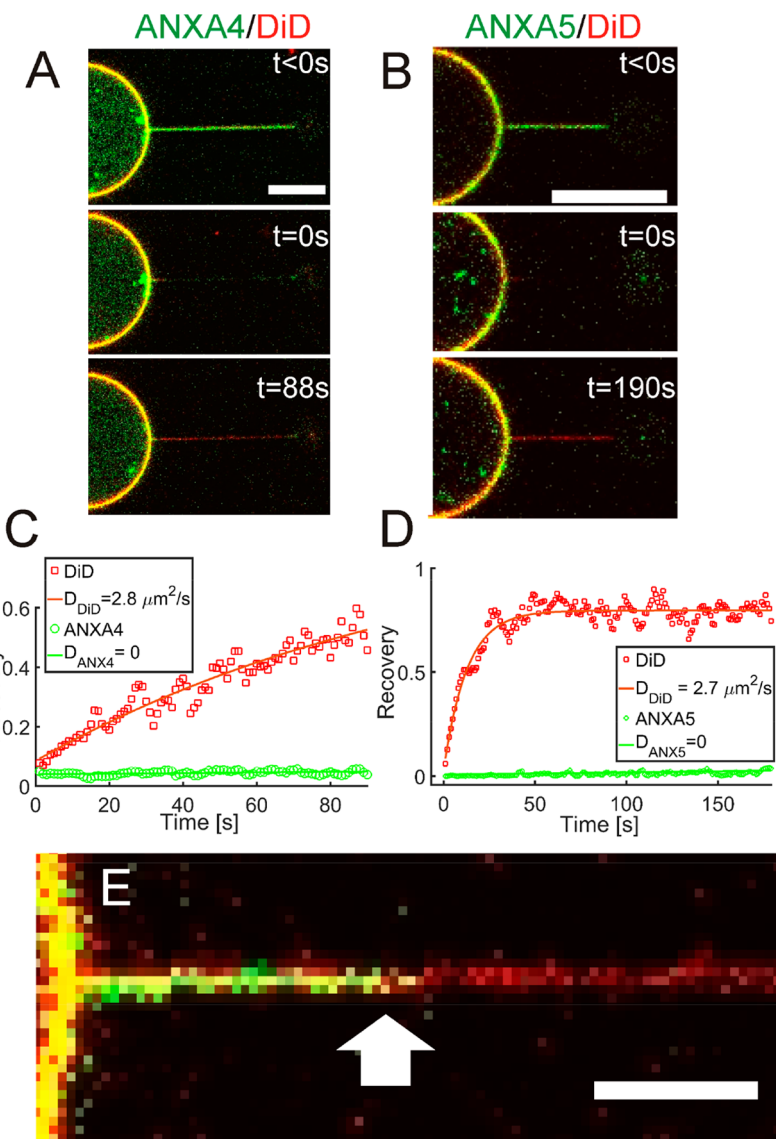


Figure 6. ANXA4 and ANXA5 have the ability to crystallize within PM nanotubes. (A) FRAP experiment on a nanotube internally coated with ANXA4-GFP and labeled with DiD. The overlaid images show no recovery of the ANXA4-GFP signal, whereas the red DiD recovers completely. (B) FRAP experiment on a nanotube internally coated with ANXA5-GFP and labeled with DiD. The overlaid images show no recovery of the ANXA5-GFP signal, whereas the red DiD recovers completely. Scale bars in (A,B) are 10 μm . (C,D) Recovery of ANXA4-GFP (C) and ANXA5-GFP (D) quantified over time. (E) Extending the bleached nanotube, containing ANXA4-GFP shows that the protein does not mix within the nanotube. Scale bar in (E) is 3 μm .

phospholipid head groups can interact with each domain of the annexin core structure.⁵⁹ Thus, it is plausible that one protein can bind to several similar or dissimilar anionic lipids in the plasma membrane. Moreover, several annexin family members, including ANXA1, ANXA2, and ANXA5, can bind to actin filaments in a Ca^{2+} -dependent manner, and this interaction may also impact their mobility and sorting.^{60–62}

To investigate if the loss in ANXA5-GFP mobility could be caused by oligomerization, we tested another member of the annexin family (ANXA4-GFP) that has also been reported to form homotrimers.⁴ Similar to ANXA5-GFP, ANXA4-GFP did not exhibit recovery even after several minutes (Figures 6A–D). Interestingly, a bleached tube containing ANXA4-GFP, with no recovery, could be further extended without causing mixing of the bleached and unbleached fraction of the tube (Figure 6E). The tendency of the proteins to become immobile within the nanotubes should only occur above a

certain density of proteins, which would be sufficient to create a connected protein network. However, the protein density in PM vesicles depends on both the fluorescently labeled and unlabeled annexins within the nanotubes and is therefore not directly accessible in our experiments. The differences in the diffusion for the three annexins are consistent with the finding that ANXA4 and ANXA5 have been reported to form trimers in ensemble studies, whereas ANXA2 was not found to trimerize,⁵⁰ which supports the idea that the lack of ANXA4 and ANXA5 recovery can be caused by lateral protein–protein contacts within the nanotubes.

The diffusion of annexins can also be affected by interactions with other proteins present in the PM vesicles. The different annexins have variable NH_2 terminal regions, which can facilitate specific interactions with cytosolic proteins, like members from the calcium-sensitive S100 protein family. S100 family members are upregulated in metastatic cells, and

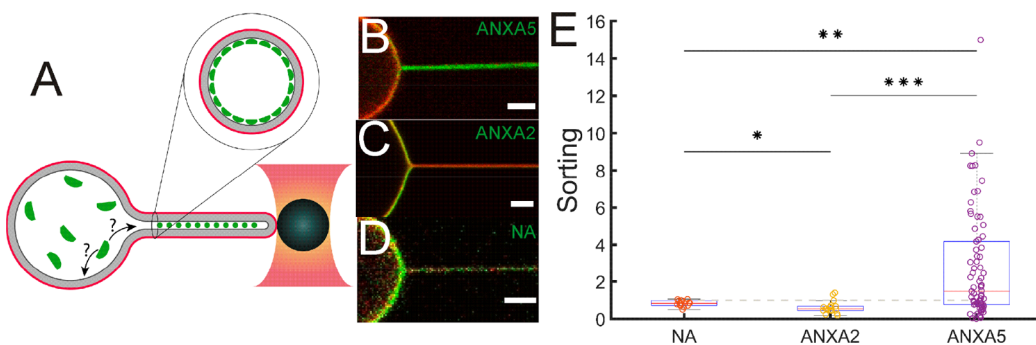


Figure 7. Membrane protein affinity for negative membrane curvature was assessed using optically extracted nanotubes from PM vesicles. (A) Schematic of the curvature assay illustrated with cytosolic annexins. The vesicle membrane provides a nearly flat reference surface compared to the highly curved nanotube. (B–D) Representative images of the nanotubes extracted from DiD labeled PM vesicles that were derived from cells expressing the indicated proteins. The degree of sorting is determined by measuring the intensity of GFP labeled proteins and the curvature insensitive lipid analogue DiD in the confocal overlays. Scale bars are 3 μm . (E) Box-and-whiskers plot showing the MC sorting that was calculated for ANXA5-GFP ($N = 74$), ANXA2-GFP ($N = 16$), and NA-GFP ($N = 16$) by comparing the values obtained at the vesicle membrane and the nanotube. A two-sample t test was used (* $p = 0.03$, ** $p = 0.01$, *** $p = 0.004$). The horizontal dashed line refers to $S = 1$, which indicates the level at which the density is the same in the tube and in the vesicle.

together with annexins they play an important role in plasma membrane repair.⁶³

Regarding the correlation between GFP intensity/protein density and mobility, we have tested if loss of mobility in a tube with higher density of labeled annexin can be obtained while mobility is still retained in the vesicle membrane from where the tube was extracted. As shown in Figure S9, a nanotube can exhibit no recovery, whereas the GFP signal recovers within seconds on the vesicle membrane. We have measured six nanotubes with immobile ANXA5-GFP in the tube and with mobile ANXA5-GFP on the vesicle membrane, and these had variable degrees of sorting. These experiments show that mobility can be retained in the vesicle, whereas the protein can become immobile in the tube, which indicates some protein interactions present in the tube only. Our experiments also contain unlabeled ANXA5 (and other types of unlabeled annexins) so therefore we cannot directly infer any relationship between density and mobility. Because mobility is different between the tube and the vesicle, it indicates that membrane curvature or interaction with other unlabeled proteins, present in the tube, plays a role in the immobilization.

Although the viral membrane protein NA was found to segregate into large-scale membrane phases, we found that it does not form molecular assemblies exhibiting slow collective diffusion, as shown by the diffusion data in Figure 5F.

Membrane Curvature Sensing of Plasma Membrane Proteins. Membrane curvature is known to affect the lateral distribution of certain membrane proteins.^{1,2,5,8,10,11} This is especially true for BAR domain proteins where a clear correlation has been observed between the convex or concave shape of the protein and the affinity for membranes with high curvature.^{8,12,13,15} However, most of these studies revealing curvature sensing have been carried out in vesicles composed of simple lipid mixtures. In addition, reconstitution of integral membrane proteins in such membranes often results in random orientation of these proteins. Because membrane proteins in PM vesicles retain their location and orientation, they provide a system that is amenable for investigating the curvature affinity of both internally encapsulated proteins and integral membrane proteins.

We therefore tested whether membrane proteins could sense the inverse membrane curvatures present within the nanotube extracted from PM vesicles (see Figure 7A). The curved shape of the membrane-binding side of ANXA5 could be a trigger for curvature-induced sorting. Here, we investigated the correlation between the ANXA5-GFP (Figure 7B) signal or ANXA2-GFP (Figure 7C) and the intensity of the curvature-insensitive DiD lipid analogue¹⁰ inside the membrane nanotube. By using the intensity on the PM vesicle membrane as a reference for both dyes, we can quantify the protein sorting, S , by the expression

$$S = \frac{(I_{\text{prot}}/I_{\text{mem}})_{\text{tube}}}{(I_{\text{prot}}/I_{\text{mem}})_{\text{vesicle}}} \quad (4)$$

S is thus a direct measure of the relative density of protein on the tube ($I_{\text{prot}}/I_{\text{mem}})_{\text{tube}}$ versus the quasi-flat surface on the vesicle, $(I_{\text{prot}}/I_{\text{mem}})_{\text{vesicle}}$.

Based on the average sorting values obtained from the analysis of ANXA5-GFP, ANXA2-GFP, and NA-GFP (Figure 7D,E) on the nanotubes extracted from the PM vesicles, ANXA2-GFP is not recruited by the high negative membrane curvature in the nanotubes as it consistently showed sorting values between 0 and 1 (Figure 7C,E). These values are slightly lower than unity ($S = 1$), which is indicative of negative sorting that effectively means ANXA2-GFP had a higher density on the flatter vesicle membrane compared to the highly curved nanotube membrane. The sorting values for NA-GFP were tightly distributed around ~ 1 , suggestive of a neutral geometric preference, which implies that NA's asymmetric morphology (due to its rather big ectodomain²⁹) does not generate a large enough imbalance to promote curvature sensing. These values also suggest that within each NA tetramer the transmembrane domains likely form a cylindrical shape,^{10,11} which is in line with a recent study showing soluble NAs fold more efficiently when a more linear tetrameric coiled-coil domain is fused to the N-terminus.⁶⁴

In contrast to ANXA2-GFP and NA-GFP, significant sorting was observed for ANXA5-GFP that ranged from strong sensing, with up to 15 times higher density ($S \sim 15$) in the tube than on the vesicle membrane, to negative ($S < 1$) sorting (Figure 7B,E).

The heterogeneity in the sorting values could be caused by variation in the protein density in the different PM vesicles, which is not known in the vesicles as both ANXA5-GFP and endogenously expressed ANXA5 can coexist in the vesicles. However, the heterogeneity was not caused by scaling of MC as no clear correlation was observed when the sorting values were plotted *versus* the relative tube diameter (Figure S10), which was determined using the linear relationship between the fluorescent DiD ratio ($I_{\text{tube}}/I_{\text{vesicle}}$)_{DiD} and the tube diameter.⁸ We note that the diameter of membrane tubes extracted from cells^{10,23} or vesicles^{8,12,13,15} depends on the membrane tension and the stiffness of the membrane. Typical values for the tube diameter in GUVs, where the membrane tension is controlled by an aspiration micropipette, range between 20 and 200 nm. Here, we did not aspirate the vesicles, and hence, the data were collected from a distribution of nanoscale tube diameters within this range.

MC is a regulator of the lateral distribution of ANXA5 studied here. Biological structures with extremely high membrane curvatures include virus envelopes, endocytic vesicles, filopodia, and caveola.¹ Investigations on model membranes have shown that MC can strongly amplify recruitment of proteins at a membrane coverage up to a few percent.^{13,15} However, the plasma membrane is known to harbor ~30 000 proteins per μm^2 , constituting an area coverage of 30–50%.^{65–67} Curvature-induced sorting has not been demonstrated at such densities in model membrane systems. Additionally, the presence of several types of curvature-sensitive proteins might significantly change the affinity of individual proteins for high MCs. Most curvature sensing studies have been carried out using model membrane systems with a controlled protein density of one protein type. Such experiments do not address the actual biological scenario with high density of various proteins in a complex plasma membrane.

Here, we provide evidence of curvature-induced sorting of ANXA5 inside membrane nanotubes of high negative membrane curvatures $\sim 1/100 \text{ nm}^{-1}$. The sorting mechanism could be related to the shape of the ANXA5 membrane-binding domain. Other curved protein domains (e.g., BAR domains) have been shown to both sense and induce membrane curvatures.^{8,12,13,15–17} However, the curvature sensing observed for ANXA2 and ANXA5 in Figure 7 is strikingly different from the sorting observed in model membrane system for BAR domain proteins. First, we see both negative sorting (lower density in the tube than on the vesicle membrane) and high sorting up to 15 times higher density inside the tube than on the vesicle membrane (see Figure 7E). Second, the PM used here contains a plethora of different proteins with a membrane coverage exceeding 5%, at which curvature sensing in model systems has been shown to vanish.^{13,15} The large heterogeneity, which is not attributed to noise, indicates that the molecular shape of the membrane-binding domain is not solely responsible for the curvature sensing. Interestingly, we do not observe membrane curvature sensing by ANXA2. Because the core membrane-binding domain of all annexins exhibits significant similarity, it is likely that the curvature sensing is related to the ability of the proteins to oligomerize, which is a property that varies among the different annexins.

Both ANXA4 and ANXA5 have been shown to form oligomers in bulk experiments, whereas ANXA2 has not been shown to oligomerize.^{50–52} The mobility of annexin clusters of

ANXA4 or ANXA5 depends on the size of these clusters, as predicted by eq 3 and Figure 5G. In the absence of recovery, as shown in Figure 6, a molecular scaffold has formed within the tube, thus preventing mixing of annexins from the tube with annexins from the vesicle. These results strongly indicate that the observed MC sensing ability of ANXA5 could be correlated with the mobility.

A tentative mechanism behind the curvature sensing observed for ANXA5 is that the trimer state, which has been detected using electron microscopy,⁵¹ exhibits a stronger affinity for negatively curved membranes than the monomeric form. Additionally, oligomerization of annexin trimers within the tube could expel other proteins from the tube. Formation of a regular lattice of proteins within the tube could displace other proteins and hence result in upconcentration of proteins, even in a relatively crowded membrane.

We note that the measured diffusion in membrane nanotubes with diameters below 100 nm may exhibit a curvature dependence as reported for proteins reconstituted in artificial GUVs.⁶⁸ The tube diameters studied here were all below the diffraction limit and spanned a factor of ~ 8 from the thinnest to the thickest tube (see Figure S10). The high membrane curvature in the thinnest tubes would lead to a decrease of the diffusion coefficient of $\sim 50\%$ according to ref 68, thus contributing to the scattering of the diffusion coefficients, as shown in Figure 5F.

CONCLUSION

Collectively, our results demonstrate that optical manipulation and confocal imaging of PM vesicles provide an excellent platform for investigating surface dynamics of membrane proteins. Both transmembrane and peripheral membrane proteins can be readily tested for mobility, phase segregation, and membrane curvature preference while exploiting the naturally preserved state of the proteins once the membranes are isolated from living cells. Here, this platform was used to reveal phase segregation of both peripheral and integral membrane proteins. Additionally, we show that annexins exhibit nontrivial membrane curvature sensing which was correlated with mobility measurements of the proteins. The possibility of isolating PM vesicles with proteins of interest, that are properly modified and localized by cells, allows for studying protein dynamics in the crowded natural environment of the plasma membrane.

MATERIALS AND METHODS

Reagents. All chemicals were purchased from Sigma-Aldrich (St Louis, MO, USA) unless otherwise specified.

Cell Culture. HEK293T cells (ATCC) were cultured in Dulbecco's modified Eagle's medium supplemented with 10% fetal bovine serum (FBS) and 50 U/mL penicillin and 50 $\mu\text{g}/\text{mL}$ streptomycin (Fisher). The cells were maintained in a humidified incubator with 5% CO_2 at 37 °C.

ANXA Expression Plasmids. Expression plasmids with turbo-GFP C-terminal tag containing human ANXA2, ANXA4, or ANXA5 cDNA were purchased from OriGene Technologies.

Design of the NA-GFP Expression Plasmid. To create an efficient NA-GFP expression plasmid, overlap cloning⁶⁹ was used to add the coding regions for GFP and a myc-His tag to the 3' end of the NA gene (GQ166659) in the mammalian expression plasmid pHW2000.⁷⁰ The coding region for the N-terminal transmembrane was optimized as previously described,⁷¹ and a Kozak consensus sequence (GCCACC) was introduced prior to the start codon. The final construct was verified by sequencing (Eurofins Genomics).

Giant Plasma Membrane Vesicle (GPMV) Isolation. For chemical induction of GPMVs, HEK293T cells were plated in Nunc 6-well plates (Nalge Nunc International, Roskilde, Denmark) coated with poly-L-lysine to keep the cells attached during the blebbing process and to minimize cell debris in solution. At 70% confluence, cells were transiently transfected and at 48 h post-transfection stained with vybrant DiD (Molecular Probes, Eugene, OR, USA), washed with GPMV buffer (10 mM HEPES, 150 mM NaCl, 2 mM CaCl₂, pH 7.4) three times, and incubated with 1 mL of GPMV buffer containing 2 mM NEM for 1.5–2 h. Upon collection, the supernatant was kept for 30 min in the incubator to let the vesicles sink, and half of the supernatant was discarded for concentrating the solution.

Nanotube Extrusion and FRAP Experiments. FRAP experiments were performed in an inverted confocal microscope Leica TCS SP5 II with a 63× (NA 1.2) water-immersion HC PL APO Leica objective (Leica Microsystems, Wetzlar, Germany) and a custom-built optical trap based on a 1064 nm laser. Tethers were pulled from GPMVs immobilized at the bottom of a coverglass (no. 1.5) (Menzel-Gläser, Braunschweig, Germany) using 5 μm polystyrene streptavidin beads (Polysciences Inc., Warrington, USA) trapped by the optical tweezers. After pulling, we waited for 5 min before bleaching in order to let the proteins diffuse and stabilize into the recently pulled tether. Bleaching was performed with a 405 nm laser for ~2 s. Time series for pre- and postbleaching were collected using the FRAP module in the LASF Leica software.

Data Analysis. All analysis was performed with custom-made Matlab scripts (The Mathworks, Inc., Natick, MA). Briefly, the signal from the tube and the vesicle were quantified, and corresponding tube-vesicle ratios were calculated. To account for bleaching during recovery, the recovery on the tube was quantified by normalizing to the signal from the vesicle. Two-sample *t* tests were quantified by a built-in Matlab function, *ttest2*. All Matlab scripts are available upon request.

GM1 Clustering with Cholera Toxin Subunit B (CTxB). Upon transfection of HEK293T cells, CTxB-Alexa Fluor 647 (Molecular Probes, Eugene, OR, USA) was added to the live-cell imaging dishes at 1 μg/mL at 37 °C for at least 2 h. Cells were incubated with GPMV buffer for blebbing, and collected GPMVs were placed on a coverglass (no. 1.5) in a home-built polydimethylsiloxane chamber in an inverted confocal microscope mounted in a custom-built cooling stage. A 40× air objective was used for imaging.

Cell Transfections and Live Imaging (NA-GFP). For transient transfection of NA-GFP, 4.5 μg of polyethylenimine (PEI) was incubated at room temperature with 1.5 μg of the NA-GFP expression plasmid in 200 μL of NaCl (150 mM) for *ca.* 20 min. The mixture was added to 10⁶ recently attached cells on a 35 mm TC-treated dish. For live imaging, PEI was replaced with 4.5 μL of TransIT-LT1 (Mirus Bio LLC), and the mix was prepared in 1 mL of OMEM (Invitrogen) containing 5% FBS. The transfection mixtures were incubated for 20 min at room temperature and then added to 2 × 10⁵ HEK293T cells seeded on a Cellview cell culture dish, 35/10 mm (Greiner Bio-One). At 48 h post-transfection, live images were captured using an inverted LSM700 confocal microscope (ZEISS) with an excitation wavelength of 488 nm. Images were generated using Zen software (v. 7.0.5.0).

Cell Transfection (ANXA). HEK293T cells were transiently transfected with the indicated plasmid using Lipofectamine LTX transfection reagent (Fischer) according to the manufacturer's protocol 24 h before they were used in experiments.

Cell Harvesting and Fractionation (ANXA). Cells grown in 150 mm dishes (1.2 × 10⁷ cells) were washed twice in 24 h post-transfection with either ANXA2-tGFP, ANXA4-tGFP, or ANXA5-tGFP in ice-cold PBS and collected by scraping in either 3 mL of homogenization buffer without Ca²⁺ (PBS 7.4, 150 mM NaCl, 200 mM sucrose, 10 mM *N*-ethylmaleimide, 1 mM EDTA, and 2× protease inhibitor (Sigma-Aldrich)) or with Ca²⁺ (PBS 7.4, 150 mM NaCl, 200 mM sucrose, 10 mM *N*-ethylmaleimide, 1 mM CaCl₂, and 2× protease inhibitor (Sigma-Aldrich)). Vesicles were generated by passing the cell suspension through a 25G needle 10 times while on ice. Nuclei and unbroken cells were removed by centrifugation (20000 g,

for 10 min at 4 °C). Supernatant was collected, and the vesicles were collected by centrifugation (20 000 g for 20 min at 4 °C). The pellet was resuspended in 150 μL of 200 μg/mL digitonin in either HBSS (+Ca²⁺) (Gibco) or HBSS (−Ca²⁺) (Gibco) and incubated on ice for 15 min prior to centrifugation (20 000 g for 30 min at 4 °C). The supernatant containing the cytosolic fraction and the pellet containing the membrane fraction were lysed in 100 or 200 μL of 2× LSB+5% DTT (Sigma-Aldrich), respectively, and boiled at 95 °C for 5 min.

Cell Harvesting and Fractionation (NA-GFP). The cells were washed at 72 h post-transfection with NA-GFP in ice-cold PBS and collected by scraping in 150 μL of homogenization buffer (PBS 7.4, 150 mM NaCl, 1 mM EDTA, 200 mM sucrose, 10 mM *N*-ethylmaleimide, and 2× protease inhibitor (Sigma-Aldrich)). Vesicles were generated by passing the cell suspension through a 27G needle 30 times while on ice. Nuclei and unbroken cells were removed by centrifugation (2000 g, 10 min at 4 °C), and the supernatant was mixed with 800 μL of 100 mM Na₂CO₃ (pH 11.3) and incubated on ice for 30 min prior to centrifugation (180 000 g, 1 h at 4 °C). The supernatant was removed and precipitated using 20% trichloroacetic acid (10 min at 4 °C). The precipitate was sedimented (20 000 g, 5 min at room temperature), washed twice in 200 μL of ice cold acetone, and resuspended in 40 μL of nonreducing Laemmli sample buffer. The pellet containing the membrane fraction was likewise resuspended in 40 μL of nonreducing Laemmli sample buffer.

NA-GFP Deglycosylation. Cells were collected at 72 h post-transfection in 150 μL of homogenization buffer by scraping and passed through a 27G needle 30 times. Nuclei and unbroken cells were removed by centrifugation (2000 g, 10 min at 4 °C), and the supernatant was adjusted to 1% *N*-dodecyl-β-D-maltoside (DDM) and 0.5% SDS. Samples were incubated for 10 min at 37 °C and deglycosylated using 20 U of PNGaseF (NEB) according to the manufacturer's protocol. After incubation for 1 h at 37 °C, an equal volume of Laemmli sample buffer containing 40 mM DTT was added.

SDS-PAGE and Immunoblotting (NA). Samples were heated to 50 °C for 10 min prior to loading on a 7% SDS-PAGE, and the proteins were transferred to a 45 μm pore polyvinylidene fluoride membrane. The membrane was stained in Amido Black 10B, and an image was taken of the total protein transferred, after which the membrane was washed briefly in dH₂O and blocked in PBS-Tween with 3% dried milk for 30 min. Membranes were rocked at 4 °C overnight with primary antibody (1:2000 mouse antimyc (9B11; Cell Signaling Technology)). The membranes were then washed (3 × 15 min in PBS-Tween 3% milk) and incubated with HRP-conjugated anti-mouse secondary antibody (1:5000 sheep anti-mouse (GE Healthcare)) for 1 h at room temperature before the final washes (3 × 5 min in PBS-Tween 3% milk, followed by 3 × 15 min in PBS-Tween). Immunoblots were developed with SuperSignal West Femto maximum sensitivity substrate (Thermo Scientific), and images were captured using an Azure C600 imager (Azure Biosystems) and the cSeries Capture Software.

Harvesting and NA Activity Assay To Determine GPMV Treatment Effect. At 48 h post-transfection, HEK293T cells transfected with NA were harvested by scraping in 100 μL of lysis buffer (0.5% DDM, 150 mM NaCl, 20 mM Tris, pH 7.4), sonicated on ice for 30 s, and the cell debris was removed by centrifugation (20 000 g, 5 min). The postnuclear supernatants were diluted five times in reaction buffer (1 mM CaCl₂, 0.1 M potassium phosphate [pH 6.0]); 10 μL of each diluted sample was mixed with 190 μL of reaction buffer containing 2 mM 2-(4-methylumbelliferyl)-α-D-N-acetylneurameric acid (Gold Biotechnology), and the resulting fluorescence, monitored with a Spectra-Max M2e, was used to determine NA activity as previously described [10.1074/jbc.M112.424150].

Immunoblotting (ANXA). Extracts were separated by SDS-PAGE using precast 4–15% gradient gels (BioRad) and blotted onto nitrocellulose membranes (BioRad) using Trans-Blot Turbo transfer system and blocked in 5% BSA. The molecular weights of proteins from the gels were evaluated using Novex Sharp Protein Standard (Invitrogen). Primary antibodies raised against human ANXA2 (1:1000 dilution, BD610069, BD Transduction Laboratories),

ANXA4 (1:200, MAB4146, R&D systems), ANXA5 (1:1000 dilution, ab14196, Abcam), and Na,K-ATPase (1:1000, 3010, Cell signaling) were used followed by appropriate horseradish peroxidase-conjugated secondary antibodies (DAKO).

ASSOCIATED CONTENT

Supporting Information

The Supporting Information is available free of charge on the ACS Publications website at DOI: [10.1021/acsnano.9b01052](https://doi.org/10.1021/acsnano.9b01052).

Formation of PM vesicles; detection of ANXA1-GFP, ANXA2-GFP, ANXA4-GFP, and ANXA5-GFP in isolated PM vesicles; extended blots for all annexins used; nanotubes pulled from PM vesicles with unbound ANXA5-GFP; localization check for ANXA5-GFP by addition of proteinase K; binding of recombinant ANXA5-GFP to the outer leaflet of PM vesicles; phase partitioning of NA in phase-separated vesicles; phase-separated PM vesicles with bound ANXA5-GFP to the internal leaflet; mobility of ANXA5-GFP on extracted nanotube and on the vesicle membrane; membrane curvature sorting of ANXA2, ANXA5, and NA *versus* relative tube diameter ([PDF](#))

AUTHOR INFORMATION

Corresponding Author

*E-mail: bendix@nbi.dk.

ORCID

Poul Martin Bendix: [0000-0001-8838-8887](#)

Author Contributions

G.M.P. and C.D.F. contributed equally. G.M.P. and E.L.V. carried out all neuraminidase experiments in PM vesicles. C.F. and A.K.S. carried out all of the corresponding experiments with ANXA5 and ANXA4, respectively. H.Ø. made all biochemical experiments relating to neuraminidase. H.Ø. and S.S. purified neuraminidase plasmids. S.L.S. performed the ANXA blots. T.L.B. purified ANXA plasmid and recombinant proteins. R.D., J.N., and P.M.B. designed and supervised the project. All authors contributed to writing and critically editing the manuscript.

Notes

The authors declare no competing financial interest.

ACKNOWLEDGMENTS

We acknowledge helpful discussions with Stanley Brown regarding the experiments. This work is financially supported by Danish Council for Independent Research, Natural Sciences (DFF-4181-00196 (to P.M.B. and G.M.P.) and 6108-00378A (to J.N.)), the Lundbeck Foundation (R218-2016-534 (to P.M.B. and C.F.)), the KV-Foundation (6030/2 (to J.N.)), the Scientific Committee Danish Cancer Society (R167-A10895-17-S2 (to J.N. and S.L.S.)), the Danish National Research Foundation (DNRF116), the Novo Nordisk Foundation (NNFOC150011361), the Swedish Research Council (to R.D.), and federal funds from the NIH–NIAID CEIRS (HHSN272201400005C (to R.D.)).

REFERENCES

- Jarsch, I. K.; Daste, F.; Gallop, J. L. Membrane Curvature in Cell Biology: An Integration of Molecular Mechanisms. *J. Cell Biol.* **2016**, *214*, 375–387.
- McMahon, H. T.; Boucrot, E. Membrane Curvature at a Glance. *J. Cell Sci.* **2015**, *128*, 1065–1070.

(3) Bassereau, P.; Jin, R.; Baumgart, T.; Deserno, M.; Dimova, R.; Frolov, V. A.; Bashkirov, P. V.; Grubmuller, H.; Jahn, R.; Risselada, H. J.; Johannes, L.; Kozlov, M. M.; Lipowsky, R.; Pucadyil, T. J.; Zeno, W. F.; Stachowiak, J. C.; Stamou, D.; Breuer, A.; Lauritsen, L.; Simon, C.; et al. The 2018 Biomembrane Curvature and Remodeling Roadmap. *J. Phys. D: Appl. Phys.* **2018**, *51*, 343001.

(4) Boye, T. L.; Maeda, K.; Pezeshkian, W.; Sonder, S. L.; Haeger, S. C.; Gerke, V.; Simonsen, A. C.; Nylandsted, J. Annexin A4 and A6 Induce Membrane Curvature and Constriction During Cell Membrane Repair. *Nat. Commun.* **2017**, *8*, 1623.

(5) Barooji, Y. F.; Rorvig-Lund, A.; Semsey, S.; Reihani, S. N. S.; Bendix, P. M. Dynamics of Membrane Nanotubes Coated with I-Bar. *Sci. Rep.* **2016**, *6*, 30054.

(6) Tsai, F. C.; Koenderink, G. H. Shape Control of Lipid Bilayer Membranes by Confined Actin Bundles. *Soft Matter* **2015**, *11*, 8834–8847.

(7) Shi, Z.; Baumgart, T. Membrane Tension and Peripheral Protein Density Mediate Membrane Shape Transitions. *Nat. Commun.* **2015**, *6*, 5974.

(8) Ramesh, P.; Barozi, Y. F.; Reihani, S. N. S.; Stamou, D.; Oddershede, L. B.; Bendix, P. M. Fbar Syndapin 1 Recognizes and Stabilizes Highly Curved Tubular Membranes in a Concentration Dependent Manner. *Sci. Rep.* **2013**, *3*, 1565.

(9) Zhao, H.; Pykalainen, A.; Lappalainen, P. I-Bar Domain Proteins: Linking Actin and Plasma Membrane Dynamics. *Curr. Opin. Cell Biol.* **2011**, *23*, 14–21.

(10) Roshholm, K. R.; Leijnse, N.; Mantsiou, A.; Tkach, V.; Pedersen, S. L.; Wirth, V. F.; Oddershede, L. B.; Jensen, K. J.; Martinez, K. L.; Hatzakis, N. S.; Bendix, P. M.; Callan-Jones, A.; Stamou, D. Membrane Curvature Regulates Ligand-Specific Membrane Sorting of Gpcrs in Living Cells. *Nat. Chem. Biol.* **2017**, *13*, 724–729.

(11) Aimon, S.; Callan-Jones, A.; Berthaud, A.; Pinot, M.; Toombes, G. E.; Bassereau, P. Membrane Shape Modulates Transmembrane Protein Distribution. *Dev. Cell* **2014**, *28*, 212–218.

(12) Zhu, C.; Das, S. L.; Baumgart, T. Nonlinear Sorting, Curvature Generation, and Crowding of Endophilin N-Bar on Tubular Membranes. *Biophys. J.* **2012**, *102*, 1837–1845.

(13) Sorre, B.; Callan-Jones, A.; Manzi, J.; Goud, B.; Prost, J.; Bassereau, P.; Roux, A. Nature of Curvature Coupling of Amphiphysin with Membranes Depends on Its Bound Density. *Proc. Natl. Acad. Sci. U. S. A.* **2012**, *109*, 173–178.

(14) Heinrich, M.; Tian, A.; Esposito, C.; Baumgart, T. Dynamic Sorting of Lipids and Proteins in Membrane Tubes with a Moving Phase Boundary. *Proc. Natl. Acad. Sci. U. S. A.* **2010**, *107*, 7208–7213.

(15) Prevost, C.; Zhao, H.; Manzi, J.; Lemichez, E.; Lappalainen, P.; Callan-Jones, A.; Bassereau, P. Irsp53 Senses Negative Membrane Curvature and Phase Separates Along Membrane Tubules. *Nat. Commun.* **2015**, *6*, 8529.

(16) Frost, A.; Perera, R.; Roux, A.; Spasov, K.; Destaing, O.; Egelman, E. H.; De Camilli, P.; Unger, V. M. Structural Basis of Membrane Invagination by F-Bar Domains. *Cell* **2008**, *132*, 807–817.

(17) Yu, H.; Schulten, K. Membrane Sculpting by F-Bar Domains Studied by Molecular Dynamics Simulations. *PLoS Comput. Biol.* **2013**, *9*, No. e1002892.

(18) Wu, Z.; Su, M.; Tong, C.; Wu, M.; Liu, J. Membrane Shape-Mediated Wave Propagation of Cortical Protein Dynamics. *Nat. Commun.* **2018**, *9*, 136.

(19) Franquelim, H. G.; Khmelinskaia, A.; Sobczak, J. P.; Dietz, H.; Schwille, P. Membrane Sculpting by Curved DNA Origami Scaffolds. *Nat. Commun.* **2018**, *9*, 811.

(20) Simunovic, M.; Prevost, C.; Callan-Jones, A.; Bassereau, P. Physical Basis of Some Membrane Shaping Mechanisms. *Philos. Trans. R. Soc., A* **2016**, *374*, 20160034.

(21) Simunovic, M.; Voth, G. A. Membrane Tension Controls the Assembly of Curvature-Generating Proteins. *Nat. Commun.* **2015**, *6*, 7219.

(22) Stachowiak, J. C.; Schmid, E. M.; Ryan, C. J.; Ann, H. S.; Sasaki, D. Y.; Sherman, M. B.; Geissler, P. L.; Fletcher, D. A.; Hayden, C. C.

- Membrane Bending by Protein-Protein Crowding. *Nat. Cell Biol.* **2012**, *14*, 944–949.
- (23) Diz-Muñoz, A.; Fletcher, D. A.; Weiner, O. D. Use the Force: Membrane Tension as an Organizer of Cell Shape and Motility. *Trends Cell Biol.* **2013**, *23*, 47–53.
- (24) Leijnse, N.; Oddershede, L. B.; Bendix, P. M. Helical Buckling of Actin inside Filopodia Generates Traction. *Proc. Natl. Acad. Sci. U. S. A.* **2015**, *112*, 136–141.
- (25) Bouter, A.; Gounou, C.; Berat, R.; Tan, S.; Gallois, B.; Granier, T.; d'Estaintot, B. L.; Poschl, E.; Brachvogel, B.; Brisson, A. R. Annexin-A5 Assembled into Two-Dimensional Arrays Promotes Cell Membrane Repair. *Nat. Commun.* **2011**, *2*, 270.
- (26) Barman, S.; Adhikary, L.; Chakrabarti, A. K.; Bernas, C.; Kawaoka, Y.; Nayak, D. P. Role of Transmembrane Domain and Cytoplasmic Tail Amino Acid Sequences of Influenza a Virus Neuraminidase in Raft Association and Virus Budding. *J. Virol.* **2004**, *78*, 5258–5269.
- (27) Calder, L. J.; Wasilewski, S.; Berriman, J. A.; Rosenthal, P. B. Structural Organization of a Filamentous Influenza a Virus. *Proc. Natl. Acad. Sci. U. S. A.* **2010**, *107*, 10685–10690.
- (28) Chlanda, P.; Schraidt, O.; Kummer, S.; Riches, J.; Oberwinkler, H.; Prinz, S.; Krausslich, H. G.; Briggs, J. A. Structural Analysis of the Roles of Influenza a Virus Membrane-Associated Proteins in Assembly and Morphology. *J. Virol.* **2015**, *89*, 8957–8966.
- (29) da Silva, D. V.; Nordholm, J.; Madjo, U.; Pfeiffer, A.; Daniels, R. Assembly of Subtype 1 Influenza Neuraminidase Is Driven by Both the Transmembrane and Head Domains. *J. Biol. Chem.* **2013**, *288*, 644–653.
- (30) Sezgin, E.; Kaiser, H. J.; Baumgart, T.; Schwille, P.; Simons, K.; Levental, I. Elucidating Membrane Structure and Protein Behavior Using Giant Plasma Membrane Vesicles. *Nat. Protoc.* **2012**, *7*, 1042–1051.
- (31) Dou, D.; da Silva, D. V.; Nordholm, J.; Wang, H.; Daniels, R. Type II Transmembrane Domain Hydrophobicity Dictates the Cotranslational Dependence for Inversion. *Mol. Biol. Cell* **2014**, *25*, 3363–3374.
- (32) Streicher, P.; Nassoy, P.; Barmann, M.; Dif, A.; Marchi-Artzner, V.; Brochard-Wyart, F.; Spatz, J.; Bassereau, P. Integrin Reconstituted in Guvs: A Biomimetic System to Study Initial Steps of Cell Spreading. *Biochim. Biophys. Acta, Biomembr.* **2009**, *1788*, 2291–2300.
- (33) Scott, R. E.; Perkins, R. G.; Zschunke, M. A.; Hoerl, B. J.; Maerklein, P. B. Plasma Membrane Vesiculation in 3t3 and Sv3t3 Cells. I. Morphological and Biochemical Characterization. *J. Cell Sci.* **1979**, *35*, 229–243.
- (34) Schafer, L. V.; de Jong, D. H.; Holt, A.; Rzepiela, A. J.; de Vries, A. H.; Poolman, B.; Killian, J. A.; Marrink, S. J. Lipid Packing Drives the Segregation of Transmembrane Helices into Disordered Lipid Domains in Model Membranes. *Proc. Natl. Acad. Sci. U. S. A.* **2011**, *108*, 1343–1348.
- (35) Levental, I.; Grzybek, M.; Simons, K. Raft Domains of Variable Properties and Compositions in Plasma Membrane Vesicles. *Proc. Natl. Acad. Sci. U. S. A.* **2011**, *108*, 11411–11416.
- (36) Levental, I.; Lingwood, D.; Grzybek, M.; Coskun, U.; Simons, K. Palmitoylation Regulates Raft Affinity for the Majority of Integral Raft Proteins. *Proc. Natl. Acad. Sci. U. S. A.* **2010**, *107*, 22050–22054.
- (37) Baumgart, T.; Hammond, A. T.; Sengupta, P.; Hess, S. T.; Holowka, D. A.; Baird, B. A.; Webb, W. W. Large-Scale Fluid/Fluid Phase Separation of Proteins and Lipids in Giant Plasma Membrane Vesicles. *Proc. Natl. Acad. Sci. U. S. A.* **2007**, *104*, 3165–3170.
- (38) Leser, G. P.; Lamb, R. A. Influenza Virus Assembly and Budding in Raft-Derived Microdomains: A Quantitative Analysis of the Surface Distribution of Ha, Na and M2 Proteins. *Virology* **2005**, *342*, 215–227.
- (39) Veit, M.; Thaa, B. Association of Influenza Virus Proteins with Membrane Rafts. *Adv. Virol.* **2011**, *2011*, 370606.
- (40) Johnson, S. A.; Stinson, B. M.; Go, M. S.; Carmona, L. M.; Reminick, J. I.; Fang, X.; Baumgart, T. Temperature-Dependent Phase Behavior and Protein Partitioning in Giant Plasma Membrane Vesicles. *Biochim. Biophys. Acta, Biomembr.* **2010**, *1798*, 1427–1435.
- (41) Nikolaus, J.; Scolari, S.; Bayraktarov, E.; Jungnick, N.; Engel, S.; Pia Plazzo, A.; Stockl, M.; Volkmer, R.; Veit, M.; Herrmann, A. Hemagglutinin of Influenza Virus Partitions into the Nonraft Domain of Model Membranes. *Biophys. J.* **2010**, *99*, 489–498.
- (42) Zhang, J.; Pekosz, A.; Lamb, R. A. Influenza Virus Assembly and Lipid Raft Microdomains: A Role for the Cytoplasmic Tails of the Spike Glycoproteins. *J. Virol.* **2000**, *74*, 4634–4644.
- (43) Melkonian, K. A.; Ostermeyer, A. G.; Chen, J. Z.; Roth, M. G.; Brown, D. A. Role of Lipid Modifications in Targeting Proteins to Detergent-Resistant Membrane Rafts. Many Raft Proteins Are Acylated, While Few Are Prenylated. *J. Biol. Chem.* **1999**, *274*, 3910–3917.
- (44) Madsen, J. J.; Grime, J. M. A.; Rossman, J. S.; Voth, G. A. Entropic Forces Drive Clustering and Spatial Localization of Influenza a M2 During Viral Budding. *Proc. Natl. Acad. Sci. U. S. A.* **2018**, *115*, E8595–E8603.
- (45) Rossman, J. S.; Jing, X.; Leser, G. P.; Lamb, R. A. Influenza Virus M2 Protein Mediates Escrt-Independent Membrane Scission. *Cell* **2010**, *142*, 902–913.
- (46) Polozov, I. V.; Bezrukov, L.; Gawrisch, K.; Zimmerberg, J. Progressive Ordering with Decreasing Temperature of the Phospholipids of Influenza Virus. *Nat. Chem. Biol.* **2008**, *4*, 248–255.
- (47) Calizo, R. C.; Scarlata, S. Discrepancy between Fluorescence Correlation Spectroscopy and Fluorescence Recovery after Photo-bleaching Diffusion Measurements of G-Protein-Coupled Receptors. *Anal. Biochem.* **2013**, *440*, 40–48.
- (48) Fujiwara, T.; Ritchie, K.; Murakoshi, H.; Jacobson, K.; Kusumi, A. Phospholipids Undergo Hop Diffusion in Compartmentalized Cell Membrane. *J. Cell Biol.* **2002**, *157*, 1071–1081.
- (49) Berk, D. A.; Hochmuth, R. M. Lateral Mobility of Integral Proteins in Red Blood Cell Tethers. *Biophys. J.* **1992**, *61*, 9–18.
- (50) Patel, D. R.; Isas, J. M.; Ladokhin, A. S.; Jao, C. C.; Kim, Y. E.; Kirsch, T.; Langen, R.; Haigler, H. T. The Conserved Core Domains of Annexins A1, A2, A5, and B12 Can Be Divided into Two Groups with Different Ca²⁺-Dependent Membrane-Binding Properties. *Biochemistry* **2005**, *44*, 2833–2844.
- (51) Oling, F.; Bergsma-Schutter, W.; Brisson, A. Trimers, Dimers of Trimers, and Trimers of Trimers Are Common Building Blocks of Annexin A5 Two-Dimensional Crystals. *J. Struct. Biol.* **2001**, *133*, 55–63.
- (52) Oling, F.; Santos, J. S.; Govorukhina, N.; Mazeres-Dubut, C.; Bergsma-Schutter, W.; Oostergetel, G.; Keegstra, W.; Lambert, O.; Lewit-Bentley, A.; Brisson, A. Structure of Membrane-Bound Annexin A5 Trimers: A Hybrid Cryo-Em - X-Ray Crystallography Study. *J. Mol. Biol.* **2000**, *304*, 561–573.
- (53) Voges, D.; Berendes, R.; Burger, A.; Demange, P.; Baumeister, W.; Huber, R. Three-Dimensional Structure of Membrane-Bound Annexin V. A Correlative Electron Microscopy-X-Ray Crystallography Study. *J. Mol. Biol.* **1994**, *238*, 199–213.
- (54) Olofsson, A.; Mallouh, V.; Brisson, A. Two-Dimensional Structure of Membrane-Bound Annexin V at 8 Å Resolution. *J. Struct. Biol.* **1994**, *113*, 199–205.
- (55) Saffman, P. G.; Delbrück, M. Brownian Motion in Biological Membranes. *Proc. Natl. Acad. Sci. U. S. A.* **1975**, *72*, 3111–3113.
- (56) Chang, M.; Kwon, M.; Kim, S.; Yunn, N. O.; Kim, D.; Ryu, S. H.; Lee, J. B. Aptamer-Based Single-Molecule Imaging of Insulin Receptors in Living Cells. *J. Biomed. Opt.* **2014**, *19*, 051204.
- (57) Guigas, G.; Weiss, M. Size-Dependent Diffusion of Membrane Inclusions. *Biophys. J.* **2006**, *91*, 2393–2398.
- (58) Knight, J. D.; Lerner, M. G.; Marcano-Velazquez, J. G.; Pastor, R. W.; Falke, J. J. Single Molecule Diffusion of Membrane-Bound Proteins: Window into Lipid Contacts and Bilayer Dynamics. *Biophys. J.* **2010**, *99*, 2879–2887.
- (59) Lizarbe, M. A.; Barrasa, J. I.; Olmo, N.; Gavilanes, F.; Turnay, J. Annexin-Phospholipid Interactions. Functional Implications. *Int. J. Mol. Sci.* **2013**, *14*, 2652–2683.
- (60) Jaiswal, J. K.; Lauritsen, S. P.; Scheffer, L.; Sakaguchi, M.; Bunkenborg, J.; Simon, S. M.; Kallunki, T.; Jaattela, M.; Nylandsted, J.

S100a11 Is Required for Efficient Plasma Membrane Repair and Survival of Invasive Cancer Cells. *Nat. Commun.* **2014**, *5*, 3795.

(61) Hayes, M. J.; Rescher, U.; Gerke, V.; Moss, S. E. Annexin-Actin Interactions. *Traffic* **2004**, *5*, 571–576.

(62) Tzima, E.; Trotter, P. J.; Orchard, M. A.; Walker, J. H. Annexin V Relocates to the Platelet Cytoskeleton Upon Activation and Binds to a Specific Isoform of Actin. *Eur. J. Biochem.* **2000**, *267*, 4720–4730.

(63) Jaiswal, J. K.; Nylandsted, J. S100 and Annexin Proteins Identify Cell Membrane Damage as the Achilles Heel of Metastatic Cancer Cells. *Cell Cycle* **2015**, *14*, 502–509.

(64) Dai, M.; Guo, H.; Dortmans, J. C.; Dekkers, J.; Nordholm, J.; Daniels, R.; van Kuppeveld, F. J.; de Vries, E.; de Haan, C. A. Identification of Residues That Affect Oligomerization and/or Enzymatic Activity of Influenza Virus H5N1 Neuraminidase Proteins. *J. Virol.* **2016**, *90*, 9457–9470.

(65) Linden, M.; Sens, P.; Phillips, R. Entropic Tension in Crowded Membranes. *PLoS Comput. Biol.* **2012**, *8*, No. e1002431.

(66) Dupuy, A. D.; Engelman, D. M. Protein Area Occupancy at the Center of the Red Blood Cell Membrane. *Proc. Natl. Acad. Sci. U. S. A.* **2008**, *105*, 2848–2852.

(67) Guigas, G.; Weiss, M. Effects of Protein Crowding on Membrane Systems. *Biochim. Biophys. Acta, Biomembr.* **2016**, *1858*, 2441–2450.

(68) Domanov, Y. A.; Aimon, S.; Toombes, G. E.; Renner, M.; Quemeneur, F.; Triller, A.; Turner, M. S.; Bassereau, P. Mobility in Geometrically Confined Membranes. *Proc. Natl. Acad. Sci. U. S. A.* **2011**, *108*, 12605–12610.

(69) Mellroth, P.; Daniels, R.; Eberhardt, A.; Ronnlund, D.; Blom, H.; Widengren, J.; Normark, S.; Henriques-Normark, B. Lyta, Major Autolysin of Streptococcus Pneumoniae, Requires Access to Nascent Peptidoglycan. *J. Biol. Chem.* **2012**, *287*, 11018–11029.

(70) Hoffmann, E.; Neumann, G.; Kawaoka, Y.; Hobom, G.; Webster, R. G. A DNA Transfection System for Generation of Influenza a Virus from Eight Plasmids. *Proc. Natl. Acad. Sci. U. S. A.* **2000**, *97*, 6108–6113.

(71) Nordholm, J.; Petitou, J.; Ostbye, H.; da Silva, D. V.; Dou, D.; Wang, H.; Daniels, R. Translational Regulation of Viral Secretory Proteins by the 5' Coding Regions and a Viral RNA-Binding Protein. *J. Cell Biol.* **2017**, *216*, 2283–2293.